MO architectures of octahedral metal clusters

Carlo Mealli*, José A. López and Yan Sun**

Istituto per lo Studio della Stereochimica ed Energetica dei Composti di Coordinazione del CNR, via J. Nardi 39, 50132 Florence (Italy)

Maria J. Calhorda

Instituto de Tecnologia Química e Biológica, R. Quinta Grande 6, Oeiras (Portugal) and Instituto Superior Ténico, Lisbon (Portugal)

(Received April 6, 1993; revised May 24, 1993)

Abstract

The paper presents a qualitative MO analysis of highly symmetrical, mostly diamagnetic octahedral metal clusters. Two classic types are considered: (i) clusters supported by face-capping ligands with general formula $M_6(\mu_3\text{-}X)_8L_6$ (X = π donor or acceptor, L = two-electron σ donor or the cyclopentadienyl anion) and a variety of electron counts; (ii) clusters with only terminal ligands, e.g. $[M_6(CO)_{18}]^{2-}$ (M = Ru, Os), Ni_6Cp_6 and the heteronuclear $Ni_2Zn_4Cp_6$, uniquely characterized by a *trans*-octahedron Ni–Ni bond. Rather than reporting another series of numerical results for compounds already widely investigated, the article surveys the MO architectures in the attempt to schematize a few distinctive roles for all the levels. The specific orbital contributions to the intra-ligand or metal–ligand or metal–metal bonding networks are determined. Almost in all of the cases, the MOs having M–M bonding/antibonding character comply with a general scheme made of interpenetrating radial, tangential, d_δ atomic orbitals. Importantly, the availability of d_δ orbitals allows, at least in cases such as the 84e species $[Mo_6(\mu_3\text{-}Cl)_8Cl_6]^{2-}$, a full correspondence between the numbers of M–M bonds and octahedral edges to be drawn. The metals need not be attributed the hypervalence which is implicit in theories (such as PSEPT) based on the analogies between metals and main group elements (i.e. only radial and tangential orbitals are involved in the octahedral skeleton bonding). It is shown that different electron populations also adapt to a generalized scheme of the interactions but that the effects on M–M bonding vary from case to case. Most of the interpretative work is empirically done with the visual aid provided by the program CACAO, which allows interactive graphing of numerical EHMO results.

Introduction

The numerous bonding theories, which have been developed for transition metal clusters, are now conveniently summarized in textbooks [1]. Most of the concepts are based on the results of MO calculations performed at all levels of sophistication. In general, the complexity of the MO picture increases with the increasing nuclearity of the cluster and also the qualitative understanding of the bonding becomes increasingly difficult. To interpret numerical results, several conceptual tools have been introduced. In addition to the principles of the Perturbation Theory [2], the constraints of the symmetry, the rules of the electron counting [3], the application of the isolobal analogies in view of the local geometry at each metal center [4], the empirical correlations between cluster topology and the electron count [5] have all proved to be valuable.

In spite of the accumulated knowledge, questions familiar to chemists like the number of metal–metal bonds, the respective roles of s, p and d orbitals, the deformational trends for various electron populations, the identification of the centers of the reactivity and so on, often remain unanswered. Usually, for mononuclear (or binuclear) metal complexes, the characterization of a few frontier MOs allows good correlations between structure and chemical bonding. Conversely for clusters, the HOMO and the LUMO alone (their identification is sometimes dubious because of the close-packing of the frontier MOs) have little effect on the compound stability (and/or reactivity), and the description of the intermetal bonding cannot be limited to the frontier levels. Most often the bonding MOs are buried in low energy bands and the geometrical parameters, by which the latter can be influenced, are hardly recognized.

*Author to whom correspondence should be addressed.

**On leave from the Department of Chemistry, University of Waterloo, Waterloo, Ont., N2L 3G1, Canada.

0020-1693/93/$6.00

Octahedral metal species have already received wide attention from the theoreticians and a plethora of numerical results is available [6]. Accordingly, the theoretical results of this paper cannot merely be an additional series of MO calculations which, by the way, are in substantial agreement with the existing ones. Rather, we wish to outline an empirical strategy to extract valuable qualitative chemical information for highly symmetric, but not less complicated clusters.

The computer package CACAO, developed in this laboratory [7], allows graphing of the relevant numerical results from EHMO calculations [8]. Walsh and Interaction diagrams as well as 3D drawings of the MOs and their components can be viewed on the computer's screen. The ease by which the calculations can be repeated and cross-checked helps to interpret the electron distribution, hence the chemical bonding. MO symmetry classifications and atomic orbital hybridizations, obtainable on a rigorous mathematical basis (see the Tensor Surface Harmonic theory, TSH and its application to clusters [9]), can be empirically derived with this type of visual analysis.

Essentially, this paper shows how the global MO architecture is describable in terms of the prevailing characters of all the levels, i.e. metal–ligand bonding/antibonding (b/a), intra-ligand b/a, metal–metal b/a, metal and/or ligand lone pairs (lp). Not necessarily, these pieces of chemical information are implicit in the commonly used electron counting rules. On the other hand, the rules themselves have a MO basis, so it is ultimately interesting to make a correlation between them and the newly gained vision of the MO architecture.

To restrict the database of the octahedral structural types*, only highly symmetric clusters, with or without face-capping ligands, are considered. Less symmetric compounds, or compounds with bridged edges or containing interstitial atoms, will be considered at a different time. Paramagnetic compounds or compounds which may undergo second order Jahn-Teller effects to avoid high spin ground states, are only marginally discussed here.

Criteria for analyzing the MO pictures

Each of the nine atomic metal orbitals is an important brick for building the MO architecture of the cluster. For the sake of simplicity, we always refer to an atom on the z axis, so that three orbitals are radial (s, p_z, d_{z^2}), four tangential (p_x, p_y, d_{xz}, d_{yz}) and two δ (d_{xy} and $d_{x^2-y^2}$). Altogether, the 54 metal orbitals are grouped and classified according to the O_h symmetry irrespective of the ligand disposition. We should point out that, throughout the paper, the MOs are referred to according to the pointgroup O_h even though the actual symmetry is lower.

Scheme 1 is convenient in order to have always handy the metal orbital symmetry combinations. Sometimes, the symmetry of a given MO and a look at its image are sufficient to establish its role. For example, the level a_{2g} (**I**), unmatchable by any ligand combination, has a clear-cut M–M antibonding character (δ^*), while the level a_{2u} (**II**) which has lobes pointing towards the centers of triangular faces is clearly used for M–L bonding (the roles would be reversed if there were edge-bridging ligands).

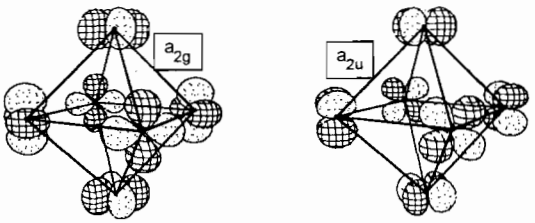

I II

An additional source of information is the electron population itself. Metal non-bonding filled combinations are obviously described as metal lone pairs, but also the simultaneous population of an M–M bonding MO and its antibonding partner can be associated with two

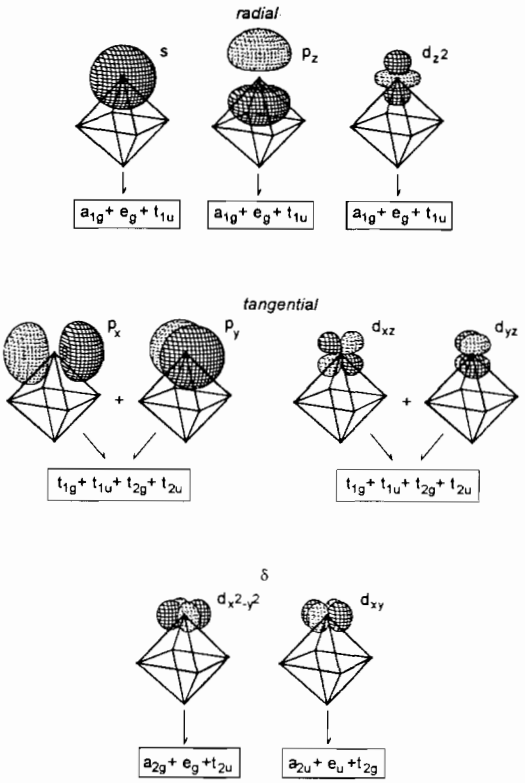

Scheme 1.

*A search in Cambridge Structural Database helped to select the compounds investigated. Some of the drawings were made by using the program PLUTO [10].

coexisting lone pairs which are somewhat repulsive to each other. As an analogy, recall the story that two electrons available to two s orbitals give rise to a H_2 molecule, whereas four electrons are only consistent with two unbonded He atoms!

Rather than assembling the naked M_6 skeleton with all of the surrounding ligands, as done by some authors [6m], it is convenient to imagine the cluster as formed by known ML_n fragments for which isolobal analogies can be invoked [4]. The Fragment Molecular Orbital analysis (FMO) [11] is then expected to highlight the origin of the M–M bonds from the frontier fragment orbitals. In any case, attention is needed, as in clusters the low lying, non-bonding FMOs may have important bonding roles [12, 13]. Other practical complications arise from the impossibility of defining the most suitable fragments for the analysis, since in some cases splitting the capping atoms in two halves would be required.

In the presence of capping ligands, a good compromise is to look at the interactions between them as a group and the metals and terminal ligands as another group. The FMO analysis usually allows the identification of the bonding interactions between the metals and the capping ligands at the first order. The subsequent evaluation of the FMOs, which are not involved in the previous interactions, provides indirect information on the M_6 bonding. Sometimes the effect of the capping ligands is also to induce second-order perturbations, hence mixings, between the metal FMOs unused for the M–L bonding network. This effect and others which are not so intuitive are best illustrated by the various examples of octahedral clusters analyzed in the paper.

Clusters of the type $M_6(\mu_3\text{-}X)_8L_6$ (X=π donor) with variable electron count

One of the most classic structures (**III**) of octahedral clusters belongs to compounds of formula $M_6(\mu_3\text{-}X)_8L_6$ (X=π donor or acceptor ligand; L=σ donor terminal ligand).

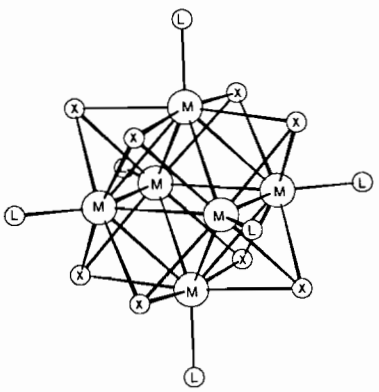

III

Notice that in the sketch as many as nine formal bonds depart from each metal atom. This does not necessarily mean that the sticks represent localized two-center/two electron bonds nor that their number in the M_6 skeleton equals the number of M–M bonds. Noticeably, for a total of 84 electrons (K) in a cluster with V metals, the Effective Atomic Number rule ($m=(18V-K)/2$) results in $m=12$ M–M bonds. In **III**, these would add to 30 total M–L and M–X bonds. Compounds such as $[Mo_6(\mu_3\text{-}X)_8Y_6]^{2-}$, X=Y=Cl [14], X=Cl, Y=OR or X=Y=OR [15], π donors, conform to this picture and are considered first.

A set of metal radial orbitals (in a first approximation formed from p_z, although some mixing is allowed, see Scheme 1) is devoted to the formation of six Mo–L_{term} bonds ($a_{1g}+e_g+t_{1u}$). In order to learn about the $Mo_6(\mu_3\text{-}X)_8$ bonding network, the symmetries spanned by the X_{capp} ligands with one σ and two π donor functions are needed, so they are summarized conveniently in **IV**. The overlap populations between FMOs confirm sufficiently good matches between the 24 X_{capp} functions and a corresponding number of isosymmetric metal combinations. For the sake of brevity, we do not show the drawings of the latter metal FMOs which are essentially formed by radial (sp hybrids), tangential (linear combinations of p_x and p_y with lobes at 45° from the main axes) and $\delta(xy)$. In general, it can be stated that M–L bonding is largely due to interactions between diffuse orbitals (s–p or p–p ones). The s–d or p–d interactions are mainly limited to the xy orbitals.

Symmetry Combinations of Capping Ligands

Radial σ	*Tangential* π
$a_{1g}+a_{2u}+t_{1u}+t_{2g}$	$e_g+e_u+t_{1u}+t_{2u}+t_{1g}+t_{2g}$

IV

The residual 24 metal orbitals (also defined as 'excess' orbitals [6h]) are used to construct the M_6 bonding network. In the local square pyramidal environment (L_5M fragments [1b]) there is a low lying σ hybrid which is largely z^2 in character. Somewhat lower, the three members of the 't_{2g}' set (reminiscent of a precursor octahedral metal complex) have tangential (xz and yz, somewhat hybridized) and d_δ (pure x^2-y^2) characters. The lobes of the latter orbital eclipse the M–M edges of the octahedron.

Certainly, the strongest interactions within the 24 'excess' orbitals involve the combinations of the radial and tangential orbitals in analogy with the bonding picture for the octahedra of non-transition elements, such as $B_6H_6^{2-}$ [3a]. The reader can find in textbooks [1b] a quick pictorial reference to the seven bonding and eleven antibonding MOs resulting from the radial+tangential mixing. Figure 1 shows an extension of this model to the δ components.

Indeed, the x^2–y^2 δ orbitals are not inert as, for the given type of local coordination, their energy matches that of the other radial and tangential components and mixing is allowed. In particular, the MOs with symmetries e_g and t_{2u} have clear-cut $\sigma+\delta$ and $\pi+\delta$ characters, respectively. As an example, **V** shows that one $2t_{2u}$ member, originally characterized by $\pi_\perp$* character, gains additional M_6 antibonding from the mixing with the two *trans*-axial δ-type orbitals. Finally, the a_{2g} MO (**I**) is most critical, because in spite of its overall M_6 antibonding character (δ*), it is relatively low in energy. The electron vacancy in this case is responsible for the 12th M–M skeletal bond. Ultimately, the a_{2g} MO features provide evidence for the active role played by δ orbitals in M_6 bonding.

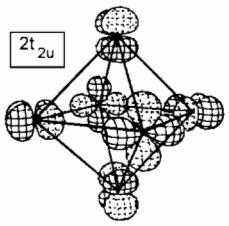

V

Importantly, 84e clusters such as $[Mo_6(\mu_3\text{-}Cl)_8Cl_6]^{2-}$ come closest to fulfilling the expectations of chemical intuition since the two sets of filled bonding and empty antibonding MOs are fully distinguishable. In fact, the number of the interatomic bonding electron pairs (30 M–L and 12 M–M) equals the number of stick bonds used for their representation (see **III**). Other common bonding descriptions, such as those based on the rules for counting the skeletal electron pairs (PSEPT theory, [6a–d]) are not equally conclusive. In fact, the ideal number of SEPs in the metal octahedral clusters should be '$7n+1$' [1a] (i.e. 86 rather than 84 valence electrons). In actuality, most closo octahedral clusters containing carbonyls conform to the ideal number of 86 electrons or, as observed by other authors [6m, n], are characterized by 43 filled cluster valence MOs (CVMOs). The latter would include all the M–L bonding pairs, a number of metal non-bonding levels and seven canonical M–M bonding pairs (SEPs).

It will be shown in the next sections, how the present MO approach can be coherently extended to well known 86e carbonyl compounds such as $[Co_6(\mu_3\text{-}CO)_8(CO)_6]^{4-}$ [16] and $Ru_6(CO)_{18}{}^{2-}$ [17]. Here, we wish to note the following. The involvement of the d_δ orbitals does not in principle ensure the full valence of the metals through an appropriate number of M–M connectivities. Hypervalence is instead implicit in theories (such as PSEPT) which are based on analogies with the main group elements (i.e. the usage of only radial and tangential orbitals is a major limitation to the description

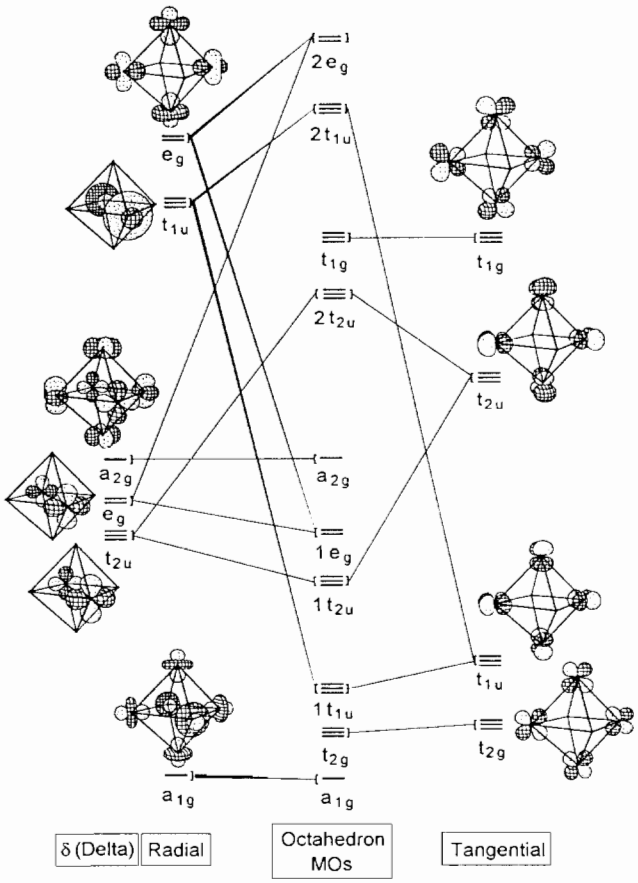

Fig. 1. A general diagram for building octahedral cluster MOs from the mutual interactions between metal components of radial, tangential and δ type. All the orbitals are in 'excess' with respect to those involved in metal–ligand interactions and altogether originate twelve bonding and twelve antibonding M–M combinations.

of the full bonding between six octahedrally arranged centers).

Now, we look at other structures of type **III** in which both the terminal ligands and the capping chalcogenides have stronger donor capabilities than the examined halides or the alkoxides. The electron count can be as low as 80e in $[Mo_6(\mu_3\text{-}X)_8(PR_3)_6]$ or 81e in the monoanion, X=S, Se [18]. Although ligand effects are important (*vide infra*), the reference MO picture is still that of Fig. 1.

In these clusters, both a_{2g} and $1e_g$ (LUMO) are empty. In agreement with previous calculations [6i], performed also at the DV-Xα level [18], the HOMO–LUMO gap is relatively large (at least 1 eV). According to Fig. 1, the $1e_g$ set should have M–M bonding character due to the in-phase combination of $\sigma+\delta$ orbitals. Now, because of their diffuseness which is responsible for a better overlap, combination of sulfur p_π orbitals mixes (*c.* 10%) and destabilizes the $1e_g$ MOs (see one component in **VI**). The M–S antibonding

character, mainly involving x^2–y^2 components, suggests that the metal $1e_g$ FMOs compete with a high e_g set to accept part of the ligand electron density. In the previous 84e case, the latter set, formed by metal p_x and p_y orbitals, was the only possible acceptor.

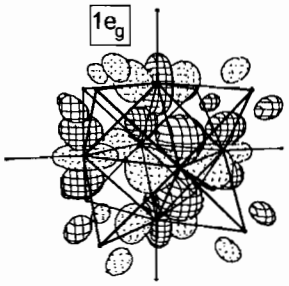

VI

Drawing **VI** confirms that the $1e_g$ MOs do not have the expected overall M–M bonding character (see Fig. 1). The two *trans* δ orbitals do still mix in a bonding fashion but the equatorial components are in a M–M antibonding relationship (horizontal rather than upright z^2-type orbitals).

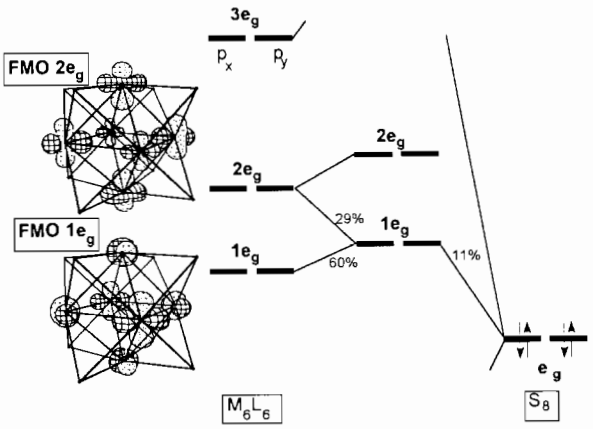

VII

The difference arises from a second-order perturbation effect which is triggered by capping chalcogenides and much less by halides or alkoxides. As shown in **VII**, the metal $1e_g$ FMOs (M–M bonding, z^2 upright) are pushed up by low S_8 FMOs whose composition can be deduced from **VI**. The upper $2e_g$ FMOs (see Fig. 1) mix in for almost 1/3 (the mixing is only half as much when the halides are involved), and thus the $1e_g$ MO acquires M–M antibonding character. From another viewpoint, the empty metal $1e_g$ FMOs compete with the higher p_x and p_y ($3e_g$) orbitals for the formation of $M–S_{capp}$ bonding. When the $1e_g$ MO set is populated (84e species) the repulsions between the electrons in the ligands p_π and those in the M–M bonding orbitals can be a source of destabilization. In this case, the halide or alkoxide capping ligands, which have more contracted orbitals, overlap less with the metal δ orbitals (only 6% of the halide contribution to $1e_g$ MOs). The overall effect, including the second order perturbation, is thus smaller and the MOs $1e_g$ can be fully populated. The diffuse chalcogenides allow the presence of, at most, a single electron in the more antibonding $1e_g$, e.g. the anion $[Mo_6(\mu_3\text{-}S)_8(PR_3)_6]^-$ [18].

The interference of the chalcogenides with the overall M_6 bonding network is also supported by the values of the Mulliken population analysis. In fact, trends in the Reduced Overlap Population indicate an increase in Mo–S bonding at the expense of Mo–Mo bonding upon the addition of four electrons to the model $[Mo_6(\mu_3\text{-}S)_8(PH_3)_6]$ ($80 \rightarrow 84$ electrons). A similar situation was previously observed [12] in M_4 planar clusters such as $[Ru_4(\mu\text{-}PPh_2)_4(CO)_{10}]$ [19]. In that case the diffuse phosphido ligands donated preferentially into some of the metal orbital combinations which were clearly important for the overall M_4 bonding framework.

As a final remark, it can be added that the $1e_g$ MOs are critical frontier levels affecting the electronic properties of the superconducting Chevrel phases and their almost pure d metal character has been emphasized [6i, 20]. Although it is not our purpose to address the point in detail, the present analysis shows that these levels are influenced by the capping ligands. Not only is the electron density in the radial $-\delta$ metal orbitals controlled by the strength of this effect, but the M–M bonding nature of $1e_g$ can be affected by the second-order perturbational effect, **VII**. It is possible that small structural rearrangements (e.g. longer $M–X_{capp}$ distances) can finely tune up the energy and nature of $1e_g$.

A structural framework very similar to that of $[Mo_6(\mu_3\text{-}S)_8(PH_3)_6]$ clusters is observed in species such as $[Co_6(\mu_3\text{-}X)_8L_6]$, X = S, Se, L = PR_3, CO, [21] which contain as many as 98 valence electrons. The latter exist also as paramagnetic monocations (97e) which recently have been investigated theoretically [22].

Our analysis exploits some of the aspects discussed up to now. Essentially, the four metal s and p orbitals plus d_{xy} are the acceptors of thirty electron pairs from the ligands. Among the 'excess' 24 orbitals (Fig. 1) only $2t_{1u}$ and $2e_g$ with prevailing radial M_6 antibonding character (hence their largest destabilization) are empty. However, if the radial character was unique there would be only one bonding partner for the five antibonding MOs, namely a_{1g}. The overall interaction would be described as a six-centers/two-electrons one and the M–M bond order would be 1/12. This is consistent with weak M_6 bonding. The overall intermetal overlap in a_{1g} must also be small in view of the long Co–Co separations of *c.* 2.8 Å and of the scarce hybridization of the radial z^2 components. However, the substantial contribution of two *trans* δ orbitals x^2–y^2 to one $2e_g$ member is confirmed (see **VIII**).

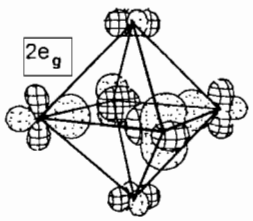

VIII

Analogously, significant tangential character appears in the $2t_{1u}$ LUMOs. Thus the overall MO architecture remains characterized by the mixing between radial + tangential + δ components and, in this light, the five empty antibonding MOs appear to have five filled bonding partners rather than a single one. The additional 14 filled levels, half bonding and half antibonding, assume the features of somewhat repelling metal lone pairs.

In a previous paper an empirical rule to calculate the numbers of M–M bonds ($=m$) and that of metal lone pairs ($=n$) in a cluster was presented [12]. The idea behind it is that each of the nine metal orbitals is either engaged in some bond or it is filled with electrons. Applied to the present case, the system of two equations (1), in which V is the total number of orbitals at the metals ($=6\times9$), L the number of metal–ligand bonds and T the total electron count, is solved for $n=14$ and $m=5$.

$$2m+n=V-L=54-30=24$$

$$2m+2n=T\text{-}2\times L=98-60=38 \qquad (1)$$

Interestingly, when applied to the 84e molybdenum species, the equations have an exact solution for $m=12$, with no lone pair since all the metal orbitals are engaged in M_6 bonding. By contrast a meaningless negative n is obtained for the 80e chalcogenide species. As was pointed out, there is no clear cut separation between the M–L and M–M frameworks in this case and the formula is not applicable in the proposed fashion.

The tetraanion $[Co_6(\mu_3\text{-}CO)_8(CO)_6]^{-4}$

The role of π-acceptor ligands at the capping positions in structures of type **III** is now explored. By considering the cluster $[Co_6(\mu_3\text{-}CO)_8(CO)_6]^{4-}$ [16], the whole band of d orbitals is two electrons short of being full. One could implicitly assume that d orbitals have a minimal role in the M–M bonding and they are, at most, responsible for a series of four electron repulsions between the metals. This case could back up the viewpoint of authors who deny the relevance of d orbitals for bonding [23]. On the other hand, Mingos and Forsyth, who first theoretically studied the cluster in question [6d], pointed out that the analogy with the boranes $B_6H_6^{2-}$ remains valid because 11 strongly antibonding combinations of radial and tangential metal orbitals can be easily individuated at high energies. Once again, recall that in main group octahedral clusters one radial and two p_π orbitals from each atom give rise to 7 bonding and 11 antibonding octahedral MOs ('$n+1$' rule).

The diagram of the interactions between the capping carbonyls and the grouping formed by metals and terminal ligands (not reported) is the tool to make empirical assignments of all the MO characters. Within the latter fragment, there are two sets of b/a MOs (symmetries $a_{1g}+t_{1u}+e_g$) which involve the σ lone pairs of terminal CO ligands and a high lying set of metal sp hybrids (1sp).

While in the case of π-donor capping ligands all of the 24 $M\text{–}X_{capp}$ bonds correspond to electron pairs which are donated to the metals, here only 8 interactions of this type are possible, the remaining bonds being attributable to metal backdonations into $\pi^*(CO)_{capp}$ levels. In Fig. 2, the arrows highlight all of the possible metal–carbonyl interactions and the sense of the electron flow. With the help of the symmetry classification of the capping ligands, given in **IV**, the one to one correspondences have been all deduced from the values of the Reduced Overlap Populations between FMOs, except for the $M\text{–}(CO)_{term}$ interactions, which are confined to the left side of Fig. 2.

Eight CO lone pairs (radial) are donated into the following empty metal FMOs:

(i) a total symmetric combination (a_{1g}) of 2sp hybrids (1sp already being used for $M\text{–}(CO)_{term}$ interactions);

(ii) two combinations ($t_{2g}+t_{1u}$) of high lying tangential p_π orbitals;

(iii) a combination (a_{2u}) of d_δ xy orbitals (see **II**).

The need for a single vacancy in the d band can be associated with the fact that only the combination in question accepts the carbonyl σ lone pairs of the same symmetry.

The backdonations into the CO π^* levels involve:

(iv) a t_{1u} combination of metal radial orbitals (z^2);

(v) $t_{2g}+e_u$ combinations of metal δ orbitals (xy); notice that xy is the only type of metal orbital being involved in both donation and backdonation;

(vi) the M_6 antibonding combination $2t_{2u}$ with mixed δ + tangential character (x^2–y^2 and xz/yz orbitals);

(vii) the M_6 antibonding combination $2e_g$ with mixed δ + radial character (x^2–y^2 and z^2 orbitals);

(viii) a tangential combination of metal d_π orbitals (t_{1g}); this corresponds to the weakest $M_6\text{–}(CO)_8$ interaction and its consequences need to be further discussed.

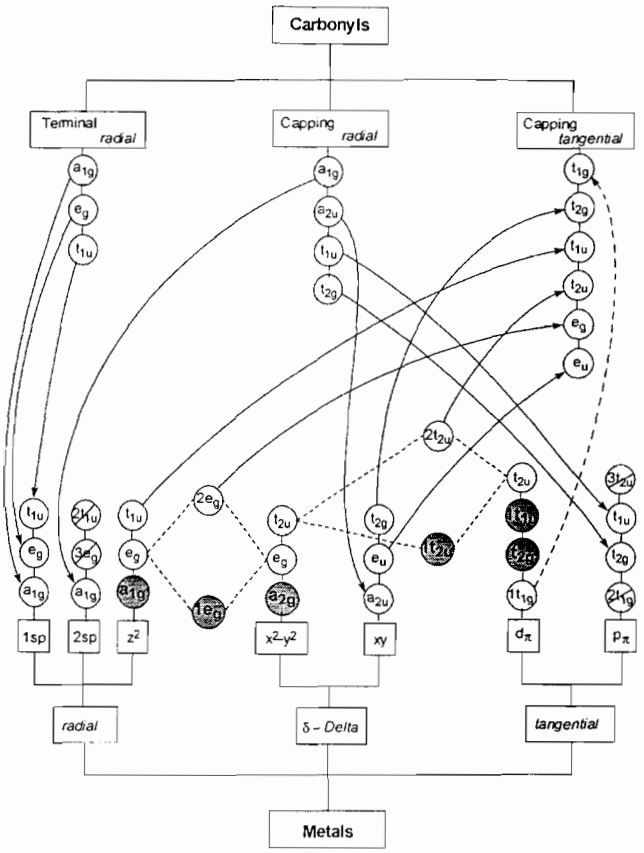

Fig. 2. A schematic representation of all the metal–carbonyl interactions in the cluster $[Co_6(CO)_{14}]^{4-}$. The arrows indicate the sense of electron flow. The dashed curve connecting the t_{1g} levels indicates a quite weak interaction. The MOs which most directly affect M_6 bonding are represented by shaded and barred spheres (populated and unpopulated levels, respectively).

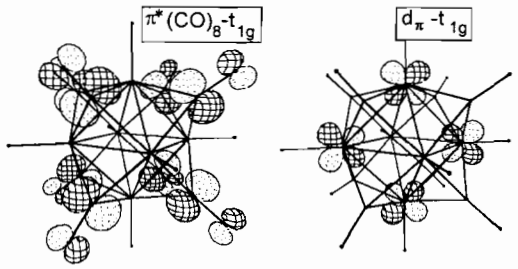

IX **X**

A visual comparison between t_{1g} members of $[\pi^*(CO)_8]$, **IX**, and metal d_π, **X**, indicates that their overlap can only be small, so it is the overlap population. The value of 0.03 is at least three/four times smaller than that for any of the other interactions. If three $M–(CO)_{capp}$ bonds do formally exist on account of the t_{1g} backdonations, they are certainly very weak (dashed connection in Fig. 2).

Evidently the FMO **IX** has a better overlap with a corresponding member of the high t_{1g} set formed by metal p_π orbitals, **XI**. In the case of capping π donors the latter is responsible for a good bonding interaction, while there are no consequences here since the FMOs **IX** and **XI** are both empty. In any case, our first assumption is that the backdonations of type t_{1g} (viii) originate three $M_6–(CO)_8$ linkages, similar to the other backdonations (iv–vii), though weaker.

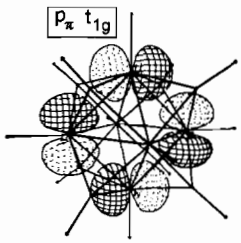

XI

As shown by the connections in Fig. 2, the electron density in $2t_{2u}$ and $2e_g$ is directed toward the carbonyls. Since the backdonation does not empty these metal levels, residual repulsions are expected with the electron pairs in the M_6 bonding partners ($1t_{2u}$ and $1e_g$). Formally, $2t_{2u}$ and $2e_g$ are used to form $M_6–(CO)_8$ bonding, while the role of M_6 antibonding partners is overtaken by the high empty p_π and 2sp metal orbitals of the same symmetry (in the case of capping π donors, the latter metal combinations are reserved for $M_6–X_8$ bonding).

In Fig. 2, twenty-four 'excess' MOs (unused for metal–ligand bonding) are easily individuated (shaded and barred circles). There is a major difference with respect to the scheme of Fig. 1: eleven M_6 antibonding MOs (all the barred circles) are now high lying combinations of sp hybrids and p_π orbitals ($e_g + t_{1u} + t_{1g} + t_{2u}$). This result is fully consistent with the indications of Mingos [6d]. The 12th M_6 antibonding level, a_{2g} (see **I**), is low lying and filled. Beside the latter, the other shaded circles indicate twelve MOs having M_6 bonding character. Among these 12 MOs, $1t_{2u}$ and $1e_g$ ensure five formal M–M bonds (the antibonding effects due to the filled $2t_{2u}$ and $2e_g$ levels are relieved by the backdonation!). It is even easier to identify the origin of the other seven M–M bonding levels, i.e. a_{1g} (z^2), t_{2g} and t_{1u} (d_π) (compare Figs. 1 and 2). Importantly, since a_{2g} is populated, the number of M–M bonds reduces to eleven and the number of lone pairs increases by two units (the filled antibonding MO wipes out one of the twelve filled bonding MOs). This is just the result of applying eqn. (1) to the 86e cluster in question ($n=2$, $m=11$).

As mentioned above, the filled $1t_{1g}$ set (d_π) is barely $M–(CO)_{capp}$ bonding. This can be a weakpoint of the above interpretation. By assuming that the $M_6–\pi^*(CO)_8$ backdonations of t_{1g}-type (**X**+**IX**) are definitely null,

not only is the total number of M–C_{capp} bonds reduced to 21, but the $1t_{1g}$ set also seems to reacquire the full M_6 antibonding character implicit in Fig. 1. Even so, there is no ultimate vanishing of as many as three M–M bonds since the major M_6 antibonding role is still played by the high lying $2t_{1g}$ combination of metal p_π orbitals (**XI**). It has been previously argued [24] that, for dimeric clusters of the type $L_3M(\mu\text{-}H_3)ML_3$ with 30 valence electrons, the M–M linkages (one σ and two π) originate from three-orbital/four-electron interactions, e.g. those corresponding to the electron configuration or $(\sigma)^2(1\sigma^*)^2(2\sigma^*)^0$ or $(\pi)^4(1\pi^*)^4(2\sigma^*)^0$. The same description seems to apply here, since 6 electrons in three of the twelve filled M–M bonding MOs (MO_{bond}) are counterbalanced by two sets of antibonding levels. Alternatively, given the configuration $(MO_{bond})^6(1t_{1g})^6(2t_{1g})^0$, **XII**, the six electrons in $1t_{1g}$ can be considered as three lone pairs, responsible for repulsive effects but not cancelling out as many as three M–M bonds*.

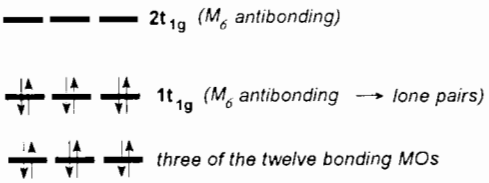

XII

As a final remark, there is no chance for the antibonding a_{2g} set to lie above all the other metal orbitals and hence to be vacant (84e species with 12 M–M bonds). This is due not only to the CO π^* orbitals which do not sufficiently push down some of the filled metal combinations (e.g. $2e_g$), but also to the strong interactions with $(CO)_{capp}$ σ lone pairs which push some of the M–M bonding MOs higher (e.g. t_{1u}, HOMO). The impossibility for a_{2g} to be empty is an intrinsic cause which constrains clusters of type $M_6(\mu_3\text{-}X)_8L_6$ to stabilize with 86e when X is a π acceptor.

Clusters of the type $M_6(\mu_3\text{-}X)_8Cp_6$

The coordination of the core $M_6(\mu_3\text{-}X)_8$ (X = π-donor) is occasionally completed by cyclo-pentadienyl anions bound in the η^5 fashion, rather than by terminal two-electron σ-donors. In particular, we refer to the known species $Ti_6(\mu_3\text{-}X)_8Cp_6$ (86e) [25] and $V_6(\mu_3\text{-}X)_8Cp_6$ (92e) [26]. In general, the six electrons contained in the π system of the Cp anion are donated to one σ or two π metal orbitals [1b], so that in these clusters as many as seven M–L bonding interactions per metal can be counted. The situation recalls that of four-legged piano-stool monomers [27] and dimers [28] in which the only non-bonding metal orbitals are of the type z^2 and x^2–y^2. In this case, the latter are the basis 'excess' orbitals, available for M_6 bonding. It is noteworthy that any pair of tangential orbitals (p_x, p_y or xz, yz: see Scheme 1) is engaged in either M–Cp or M–X_{capp} bonds and the MOs t_{2g}, $1t_{1u}$, $2t_{2u}$ and $1t_{1g}$, are now dismissed from the most complex M_6 bonding network of Fig. 1.

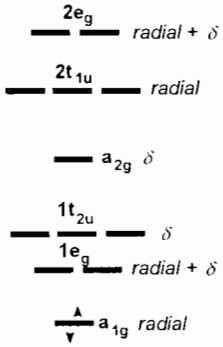

XIII

Consistent with the previous studies [6h], the 'excess' metal orbitals give rise to the twelve frontier levels, schematized in **XIII**. A unique electron pair populates the overall bonding MO a_{1g} thus suggesting an M–M bond order of 1/12. In the somewhat analogous case of the 98e species $[Co_6(\mu_3\text{-}S)_8L_6]$, additional sources of M_6 bonding could be pointed out. Although the M_6 cementing force seems here to be exclusively due to the two electron/six centers interaction of radial type, further considerations are appropriate.

First, the unavailability of tangential orbitals renders any extension of the '$n+1$' rule totally inadequate to describe the intermetal bonding network, and the fact that the cluster possesses the canonical 86 electron count (43 electron pairs) seems almost casual. Also, the EAN rule predicts an illogical number of M–M bonds (11) as does the extension of the latter (eqn. (1)). Once again, the species is ill-behaved with respect to the common counting rules because two independent M–L and M–M networks cannot be delimited. We have reached such a conclusion on the basis of the following arguments.

The whole set ($t_{2u} + e_g + a_{2g}$) of empty δ orbitals (x^2–y^2) could appear to have no role in either M–L or M–M bonding. However, the FMO analysis of the interactions between the groups M_6Cp_6 and $(\mu_3\text{-}O)_8$ shows that the x^2–y^2 orbitals are not innocent. While the higher a_{2g}

*Equations (1), applied by considering that the total number of M–L bonds is 27 rather than 30 and that the electrons involved in M–L bonding is 54 rather than 60, provide the solution $m = 11$, $n = 5$.

is uniquely unmatched, the $1e_g$ and $1t_{2u}$ combinations are somewhat destabilized by p_π combinations of the capping oxygen atoms such as that in **XIV** (two Cp rings are omitted for clarity). In addition, $1t_{2u}$ is not stabilized by mixing with tangential orbitals. Hence the order $1e_g < 1t_{2u}$ is reversed with respect to Fig. 1. As in the 80e species $[Mo_6(\mu_3\text{-}X)_8(PR_3)_6]$ (see **VI**), $1e_g$ is the LUMO and the x^2–y^2 orbitals are seen to enter into competition with the higher metal p_π orbitals to receive electron density from the capping oxygen atoms. Moreover, a second-order perturbation effect, as in **VII**, introduces M–M antibonding character into $1e_g$ via a mixing with the higher set $2e_g$ (the percentages being 60 and 22%, respectively).

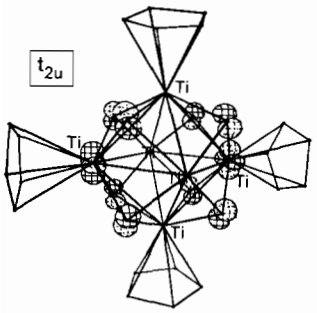

XIV

The destabilization of both $1e_g$ and t_{2u} due to the aforementioned effects, favors a relatively large HOMO–LUMO gap (>1 eV) and the 86e titanium compound acquires thermodynamic stability. On an absolute energy scale, the LUMOs are somewhat high (*c.* −10 eV) but the gap with respect to the next empty level (a_{2g}) is also large (>1 eV). The levels $1e_g$ and $1t_{2u}$ could be potentially populated with a maximum of 10 electrons. The species $V_6(\mu_3\text{-}O)_8Cp_6$ is known although only some of its derivatives such as $V_6(\mu_3\text{-}O)_8(O)Cp_5$ or the dimer $[V_6(\mu_3\text{-}X)_8Cp_5]_2O$ have been structurally characterized [26]. The five or six electrons added to the original MO structure of $Ti_6(\mu_3\text{-}O)_8Cp_6$ MO are not fully paired. In particular, the paramagnetism of the 92e species $V_6(\mu_3\text{-}O)_8Cp_6$ seems to confirm $1e_g$ as the first accessible level with a not much higher $1t_{2u}$ level. Given the limits imposed on the present qualitative discussion, we avoid any further interpretation of the magnetic aspects and of the deformational trends induced by the probable second-order Jahn-Teller effects.

Clusters having only terminal ligands

Sometimes the M–M bonding interactions are few in number and rather weak so it is questionable whether the capping ligands are a major source of stabilization for the M_6 octahedral framework. Such a doubt does not exist for clusters which have only terminal ligands. Among these, we will consider three prototypes assembled from six deltahedral metal fragments. The sample models are $M_6(CO)_{18}^{2-}$ (M = Os, Ru) [29], diamagnetic with 86e, $Ni_6Cp_6^{0,1+}$ [30], both paramagnetic with 90e and 89e, respectively, and $Ni_2Zn_4Cp_6$ [31], diamagnetic (the 98e count which includes the electrons of the zinc 3d shell is however questionable (*vide infra*)). The latter Cp species can be somehow related to the previous clusters $M_6(\mu_3\text{-}O)_8Cp_6$ (M = Ti, V) upon the removal of the O_{capp} atoms.

The six basic frontier orbitals of L_3M and CpM fragments are well known [1b]. All together, the combinations of the high lying σ hybrid, two hybridized d_π orbitals and three low lying 't_{2g}' orbitals represent 36 'excess' orbitals (ligand-free or unused for M–L bonding) which host 50 electrons in the case of $Ru_6(CO)_{18}^{2-}$, **XV** [17]. The solution of eqn. (1) (11 M–M bonds and 14 lone pairs) is a useful guideline to analyze the different MO roles in the latter species. If four M–M bonds have to depart from each metal, the orbitals potentially involved are: two tangential d_π, one δ (x^2–y^2, 't_{2g}') and one radial (either sp hybrid or z^2) orbitals.

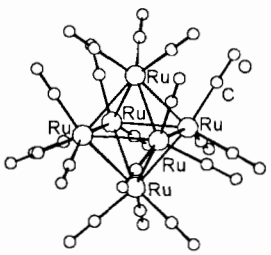

XV

Six cluster lone pairs correspond to the combinations of the *xy*-'t_{2g}' orbitals (previously involved in M–X_{capp} interactions) while the assignment of the other eight lone pairs is more tricky. Were the radial contribution to M_6 bonding fully satisfied by sp hybrids, the combinations of the z^2 ('t_{2g}') orbitals could be described as six lone pairs. Finally, two extra lone pairs are counted because of the filled M_6 antibonding MO (a_{2g}) which nullifies one of the lower bonding MOs. Although not too far from a satisfactory explanation, the previous picture which denied a M_6 bonding role to the radial z^2 orbitals is too simplistic. In fact, although the sp hybrids form the highest and very important overall radial bonding MO ($2a_{1g}$), they are too high in energy to be involved in the radial + tangential and radial + δ mixings which are beneficial for the M_6 bonding (Fig. 1). Conversely, the z^2 orbitals, degenerate with x^2–y^2 (t_{2g}) and not too far from d_π orbitals, are present in

the radial + δ and radial + tangential combinations. Scheme **XVI** summarizes the situation (for sake of clarity, the filled combinations of *xy* orbitals have been dismissed).

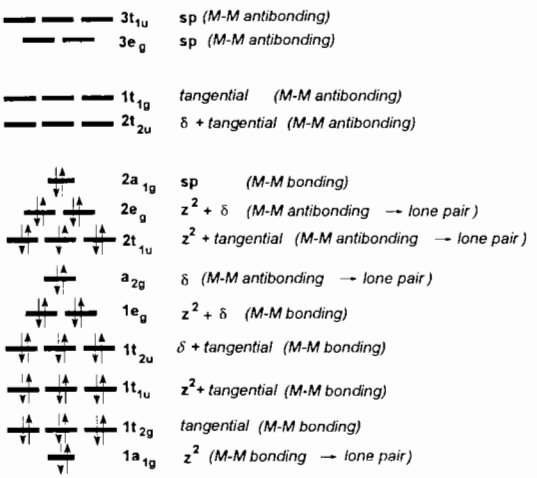

XVI

As in Fig. 1, the well hybridized d_π orbitals (*xz*, *yz*) form pure tangential t_{2g} and t_{1g} b/a combinations. They also form with the x^2–y^2 orbitals b/a combinations of t_{2u} symmetry (δ + tangential). The often underestimated role of δ orbitals in M_6 bonding can be highlighted, in this case, by an *ad hoc* FMO analysis. In fact, upon the interaction between the equatorial fragment $Ru_4(CO)_{12}$ and the group of *trans*-axial metals, $(CO)_3Ru...Ru(CO)_3$, the $\pi_\perp{}^*$ equatorial combination of d_π orbitals (see the FMO t_{2u} at the right side of Fig. 1) is destabilized *c* 0.7–0.8 eV by the corresponding δ combination (left side). Moreover, the reduced overlap population between the corresponding FMOs is significantly large ($\geqslant 0.1$).

As mentioned, the M_6 bonding MOs which involve radial + tangential and radial + δ mixings have z^2 contributions and correspond to the levels $1t_{1u}$ and $1e_g$. The situation is complicated by the corresponding antibonding levels ($2t_{1u}$ and $2e_g$) which are also filled. However, the presence of the empty high levels made of the sp hybrids ($3t_{1u}$ and $3e_g$) confers the expected bonding character to the lowest bonding sets. Previously (see **XII**) we have described situations of this type as three-orbitals/four-electron bonding, the corresponding configurations being in this case $(1t_{1u})^6(2t_{1u})^6(3t_{1u})^0$ and $(1e_g)^4(2e_g)^4(3e_g)^0$. The intrinsic weakness of this type of bonding is consistent with the viewpoint that the intermediate filled levels $2t_{1u}$ and $2e_g$ are lone pairs and thus the source of electronic repulsions. Somewhat differently and more analytically, the six z^2 combinations are assigned lone pair characters. The final number of metal lone pairs comes out to be 14, anyway.

Finally, it is highly improbable that the a_{2g} (pure δ in character) is higher than $2a_{1g}$ (HOMO) whose components are highly energetic. For this intrinsic reason, M_6L_{18} octahedral clusters (formed by conical metal fragments) stabilize with 86 electrons. As remarked by others [32], if two electrons are missing, as in the 84e case of $Os_6(CO)_{18}$ [33], other skeletal geometries are sought which allow the formation of twelve effective M–M bonds, e.g. the bicapped tetrahedron.

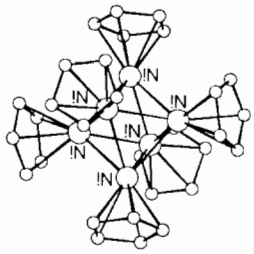

XVII

The MO pattern for the clusters $Ni_6Cp_6{}^{+1,0}$ (89, 90e) [30], **XVII**, is similarly framed, the difference being that three or four additional electrons are hosted in the $2t_{2u}$ MOs (see **XVI**). Since the precise nature of the latter orbitals raised the legitimate curiosity of the original authors [30], we attempt a qualitative description here.

First the ligand contribution prevails over that from the metal (60 versus 40%) and, apparently, the M_6 antibonding character is not enough to intolerably destabilize the level. On the other hand, the direct visualization of metal components in one $2t_{2u}$ member (**XVIII**) is not sufficient to clarify the role of these levels relative to the M_6 bonding interplay. Nor is it clear whether the expected tangential + δ mixing is still featured. Fortunately, the analysis of the Ni_6 skeletal components (upon interaction with all the Cp rings) allows a better understanding (see **XIX**).

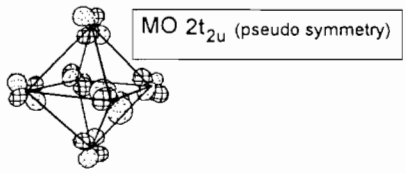

XVIII

On descending from O_h symmetry, the three Ni_6 FMOs of $2t_{2u}$ symmetry mix together so as to adopt the sterically favoured orientations of the Cp ligands. While it becomes clear that the tangential + δ mixing is still present, the orbital reorganization seems to partially quench the M_6 antibonding nature of $2t_{2u}$ (**XIX**) so that the octahedral structure is essentially preserved even in the presence of three or four electrons.

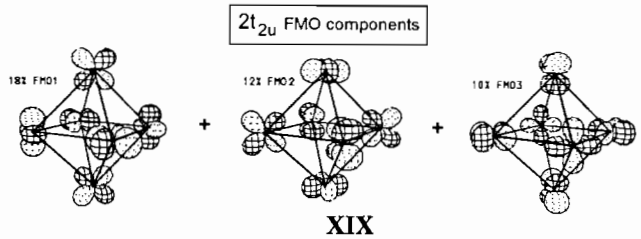

XIX

As mentioned, we are not committed to study the deformational effects induced by the uneven population of $2t_u$ in $Ni_6Cp_6^0$.

In the heteronuclear cluster $Ni_2Zn_4Cp_6$, **XX**, for which other MO calculations are available [31], the octahedral structure is only a reminiscence. In fact, a *trans*-axial Ni–Ni bond squashes the M_6 skeleton and any potential equatorial bonding between Zn atoms seems lost. Still, we find it interesting to describe the intermetal bonding network in terms of the basic radial + tangential + δ mixings between the metal orbitals. In particular, the origin of the well defined *trans*-octahedron Ni–Ni linkage (2.571(2) Å) can be tracked down.

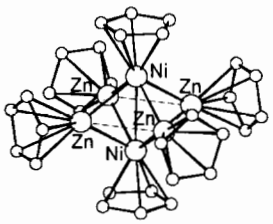

XX

Each Zn atom uses only the s and p orbitals for bonding, since the 3d orbitals are too low in energy and are largely excluded from any significant interaction. Thus, although the cluster can be counted as a 98e species, no Zn δ function participates in the Zn_4Ni_2 bonding interplay. A FMO analysis, aimed at detecting Zn–Cp interactions, shows that the cyclopentadienyl anion acts almost as a two electron donor to a Zn radial p orbital. The expected donations from the two singly noded Cp $\pi_\perp$ orbitals [1b] into two tangential Zn p_π orbitals are very small. One of the latter orbitals ($p\pi_\perp$ with respect to the Zn_4 plane) is definitely involved in the formation of Zn–Ni bonds, while the other (in the Zn_4 plane) stays unperturbed at high energy. Ultimately, this seems almost a case of three-coordination, not unusual for d^{10} metals, with one Cp–Zn and two Ni–Zn linkages.

Figure 3 is based on the original diagram produced by the program CACAO and shows the interaction between the fragments Cp_4Zn_4 (left side) and Cp_2Ni_2 (right side). For sake of clarity, only the levels relevant to the M–M bonding network are shown. The combined in-phase and the out-of-phase frontier orbitals of two facing CpNi fragments are in the order six 't_{2g}' levels, four d_π ones and a σ–σ^* pair of sp hybrids. As mentioned, the Zn atoms provide only combinations of the $p\pi_\perp$ (tangential, upright) and radial (essentially s) orbitals. The strongest interactions between the FMOs are numerically reported ($\times 1000$) in Fig. 3. Accordingly, 8 Ni–Zn bonds appear to arise from 4 interactions of the type $\sigma(Zn_4)/2\sigma(Ni_2)$, $\pi_\perp(Zn_4)/1\sigma^*(Ni_2)$, $\sigma^*(Zn_4)/\delta(Ni_2)$, $\pi_\perp(Zn_4)/\delta^*(Ni_2)$ and by 2+2 interactions of the type $n\pi_\perp(Zn_4)/\pi^*(Ni_2)$ and $n\sigma(Zn_4)/\pi(Ni_2)$. Notice that the $\sigma(Zn_4)$ overall radial combination is low in energy and can be assigned the two electrons donated to $2\sigma(Ni_2)$. Accordingly the fragment itself is formulated as $[Zn_4Cp_4]^{2+}$. In turn the Ni atoms, assigned d^{10} configurations in the fragment $[Ni_2Cp_2]^{2-}$, are able to donate seven electron pairs to the zinc atoms.

Importantly, from the two original $\sigma+\sigma^*$ couples of Cp_2Ni_2, only the lower $1\sigma^*$ (filled) and the higher 2σ (empty) FMOs get involved in Ni–Zn bonding. There remains a couple of filled and empty levels, namely 1σ and $2\sigma^*$, which is therefore responsible for a two-electron-two-center Ni–Ni bond. This recalls the case of the dimer $Fe_2(CO)_9$ for which the existence of the direct Fe–Fe σ bond has been questioned by many authors because of a slightly negative Fe–Fe overlap population [13]. Also in that case, after accounting for all the bonding components between the two iron atoms and the three bridging carbonyls, a low filled σ MO was indirectly seen to match with a high lying and empty σ^* partner. Since the Fe–Fe overlap population is the result of all the intermetallic interactions, its negative value is attributable to prevailing repulsions between d_π orbitals through the bridging ligands. The viewpoint is confirmed by calculations at the *ab initio* level [34]. Although in $Ni_2Zn_4Cp_6$ the M–M overlap population is positive (c. 0.02), a bond which involves mainly low lying, unhybridized 't_{2g}' orbitals (z^2) is not expected to be strong in any case.

The Ni–Zn interactions, described above, could also be tracked down as a part of the overall radial + tangential + δ pattern of Fig. 1. Two orbitals from each Zn atom (one p_π and one δ) are incapable of playing an active role. Conversely, four Ni–Zn bonds can depart from each Ni atom because the required set of four orbitals (one radial, two tangential and one $\delta(x^2-y^2)$) is available and can be properly exploited. In addition, each Ni carries extra $\delta(xy)$ and radial (σ) orbitals. While the δ and δ^* combinations (see Fig. 3) are counted as lone pairs, it has been shown that the σ orbitals get organized to give a direct Ni–Ni bond.

As a final consideration, the solutions of eqn. (1) obtained by introducing 54 metal orbitals and 98 electrons seem inconsistent with the existence of the nine M–M predicted by the previous analysis. The results

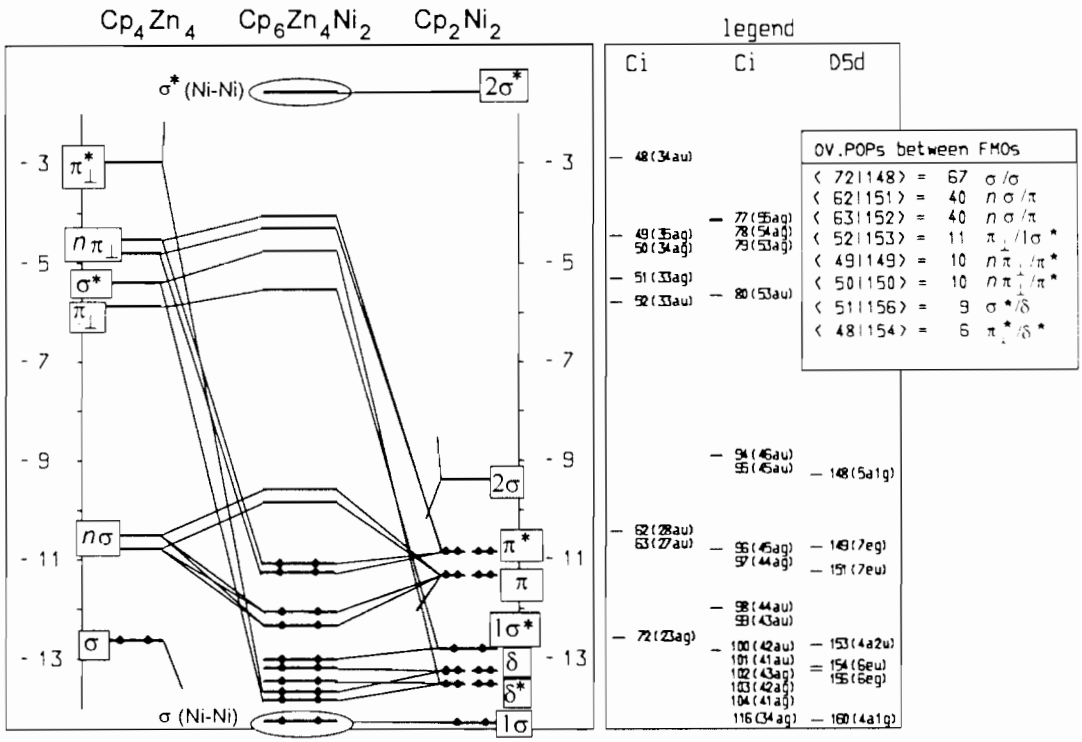

Fig. 3. The diagram, based on an original CACAO drawing, shows the interactions between the FMOs of Cp_4Zn_4 and Cp_2Ni_2 in the cluster $Cp_4Zn_4Ni_2$. For the sake of clarity, many levels with prevailing Cp character have been omitted. The label *n* characterizes FMOs which in Cp_4Zn_4 are non-bonding because they are centered on *trans*-axial Zn atoms. The reported values of the overlap population between FMOs (×1000) are the most significantly positive and suggest the formation of eight Ni–Zn bonds. The coexistence of a low filled and high empty MOs, having Ni–Ni σ and σ^* characters, accounts for a direct bond between the two Ni atoms.

become more consistent ($m = 9$ and $n = 22^*$) if the hints provided by the MO analysis are properly taken into account. Since a Cp ring donatcs only two electrons to the corresponding Zn atom and a total of four Zn p_π orbitals remain unused, the proper values for the variables T and V are 72 and 50, respectively.

Conclusions

A selection of well known octahedral metal clusters has been considered from the point of view of the MO structure. The results are generally in agreement with other calculations but the qualitative M_6 bonding network is seen under the light of the roles singularly played by all the MOs. Although many technical details need to be focused on, the interpretational task is facilitated by the systematic molecular fragmentations and by the visualization of the numerical results aided by computer graphics.

*The number of lone pairs is given by the globality of zinc filled d orbitals plus the δ and δ^* combinations of the nickel atoms unused for bonding (see Fig. 3).

In summary, the knowledge of the whole MO architecture is the actual key to understanding complicated molecules such as clusters. The various electron counting rules are useful guidelines for a general classification of the cluster typology, but only a detailed evaluation of the MOs, and of the effects of the electrons in them, can fully account for the chemical bonding and its consequences on structure and properties.

A major point is that the metal basis set, which includes δ orbitals, offers more bonding capabilities than the basis set of main group elements. Thus, in the octahedral clusters of the latter elements, each atomic component is clearly affected by hypervalence, whcreas thc concept is unnecessary for the metal species. In fact, the availability of enough orbitals (one radial, two tangential and a δ one) allows in principle each metal to have as many different interactions with neighbours as the number of edges departing from it. In order to transform all the interactions into bonds, the appropriate number of electrons must populate only the bonding MOs. Excess electron pairs, which often populate some M_6 antibonding MOs, not only delete an equivalent number of bonds but are the source of destabilizing repulsions with the electrons in the bonding levels. The reduced number of M–M bonds is thus

attributable to the vanished bonding pairs which transform into lone pairs and not to the lack of the appropriate atomic orbitals. Also, there are cases in which the orbitals good for M–M bonding are used by ligands or in which the M–L and M–M bonding frameworks clearly compete for the same orbitals.

In conclusion, the determination of the formal M–M bond order can only be evaluated after a sufficient knowledge of the electron distribution is acquired through *ad hoc* MO studies. In any case, a bond order of 7/12 (as in main group octahedral clusters) is not general for metal species and it cannot be used as a rulc of thumb.

Many of the ideas, now applied to octahedral clusters, have been built up progressively for dimeric [13, 24, 28, 34, 35], trimeric [36] and tetrameric clusters [12, 37]. Extensions to other hexameric clusters (including octahedral M_6 skeletons with asymmetric ligand disposition) and species of higher nuclearity are planned.

Calculations of the Extended Hückel type were carried out using a modified version of the Wolfsberg-Helmholz formula [38]. The geometrical parameters of the clusters investigated were as close as possible to the reported crystal structures. Atomic parameters used in the various calculations are those collected with all of the proper references by S. Alvarez in a precious booklet which can be obtained from the author upon request [39].

Acknowledgements

The work has been partially supported by the Progetto Finalizzato Chimica Fine II (C.N.R.). The work of J.A.L. c/o I.S.S.E.C.C.-C.N.R. (Firenze) has been made possible thanks to a scholarship of the Ministerio de Educación y Ciencia of the Spanish Government and that of Y.S. thanks to the encouragement and generous support of her Ph.D. advisor, Professor A. Carty (University of Waterloo). M.J.C. thanks the Direzione Progetto Finalizzato Chimica Fine II for financing a visit to Florence and JNICT for financial support (PMCT/C/CEN/367/90). Thanks are due to Professor R. Hoffmann (Cornell University) and to Dr D.M. Proserpio (Università di Milano) for their critical reading of the manuscript and to Dr G. Bianchini (I.S.S.E.C.C.) for the initial encouragement.

References

1 (a) D.M.P. Mingos and D.J. Wales, *Introduction to Cluster Chemistry,* Prentice-Hall, Englewood Cliffs, NJ, 1990; (b) T.A. Albright, J.K. Burdett and M.-H. Whangbo, *Orbital Interactions in Chemistry,* Wiley, New York, 1985.
2 R. Hoffmann, *Acc. Chem. Res., 4* (1971) 1, and refs. therein.
3 (a) K. Wade, *J. Chem. Soc., Chem. Commun.,* (1971) 792; (b) *Adv. Inorg. Chem. Radiochem., 18* (1976) 1; (c) D.M.P. Mingos, *Nature (London), Phys. Sci., 236* (1972) 99; (d) *Acc. Chem. Res., 17* (1984) 311; (e) S.M. Owen, *Polyhedron, 7* (1988) 253.
4 (a) R. Hoffmann, *Angew. Chem., Int. Ed. Engl., 21* (1982) 711; (b) D.G. Evans, *J. Chem. Soc., Chem. Commun.,* (1983) 675.
5 B.K. Teo, *Inorg. Chem., 23* (1984) 1251.
6 (a) F.A. Cotton and T.E. Haas, *Inorg. Chem., 3* (1964) 10; (b) L.J. Guggenberger and A.W. Sleight, *Inorg. Chem., 8* (1969) 2041; (c) D.M.P. Mingos, *J. Chem. Soc., Dalton Trans.,* (1974) 133; (d) D.M.P. Mingos and M.I. Forsyth, *J.Chem. Soc., Dalton Trans.,* (1977) 610; (e) D.W. Bullett, *Phys. Rev. Lett., 39* (1977) 644; (f) F.A. Cotton and G.G. Stanley, *Chem. Phys. Lett., 58* (1978) 450; (g) B.E. Bursten, F.A. Cotton and G.G. Stanley, *Isr. J. Chem., 19* (1980) 132; (h) F. Bottomley and F. Grein, *Inorg. Chem., 21* (1982) 4170; (i) T. Hughbanks and R. Hoffmann, *J. Am. Chem. Soc., 105* (1983) 1150; (j) R.L. Johnston and D.M.P. Mingos, *Inorg. Chem., 25* (1986) 1661; (l) M.H. Chisholm, D.L. Clark, M.J. Hampden-Smith and D.H. Hoffman, *Angew. Chem., Int. Ed. Engl., 28* (1989) 432; (m) J.W. Lauher, *J. Am. Chem. Soc., 100* (1978) 5305; (n) G. Ciani and A. Sironi, *J. Organomet. Chem., 197* (1980) 233.
7 C. Mealli and D.M. Proserpio, *J. Chem. Educ., 67* (1990) 399.
8 (a) R. Hoffmann, *J. Chem. Phys., 39* (1963) 1397; (b) R. Hoffmann and W.N. Lipscomb, *J. Chem. Phys., 36* (1962) 2179; (c) *36* (1962) 2872.
9 (a) A.J. Stone, *Mol. Phys., 41* (1980) 1339; (b) *Inorg. Chem., 20* (1981) 563; (c) R.L. Johnstone and D.M.P. Mingos, *Theor. Chim. Acta,* (1989) 75; (d) A. Ceulemans and P.W. Fowler, *Inorg. Chim. Acta, 10* (1985) 75.
10 F.H. Allen, J.E. Davies, J.J. Galloy, O. Johnson, O. Kennard, C.F. MacRae, E.M. Mitchell, G.F. Mitchell, J.M. Smith and D.G. Watson, *J. Chem. Inf. Comp. Sci., 31* (1991) 187.
11 (a) R. Hoffmann, H. Fujimoto, J.R. Swenson and C.C. Wan, *J. Am. Chem. Soc., 95* (1973) 7644; (b) R. Hoffmann and H. Fujimoto, *J. Phys. Chem., 78* (1974) 1167.
12 (a) C. Mealli and D.M. Proserpio, *J. Am. Chem. Soc., 112* (1990) 5484; (b) *Mater. Chem. Phys., 29* (1991) 245.
13 C. Mealli and D.M. Proserpio, *J. Organomet. Chem., 386* (1990) 203.
14 L. Ouahab, P. Batail, C. Perrin, C. Garrigou-Lagrange, *Mater. Res. Bull., 21* (1986) 1223.
15 M.H. Chisholm, J.A. Heppert and J.C. Huffman, *Polyhedron, 3* (1984) 475.
16 V. Albano, P.L. Bellon, P. Chini and V. Scatturin, *J. Organomet. Chem., 16* (1969) 461.
17 M.R. Churchill and J. Wormald, *J. Am. Chem. Soc., 93* (1971) 5670.
18 (a) T. Saito, N. Yamamoto, T. Yamagata and H. Imoto, *J. Am. Chem. Soc., 110* (1988) 1646; (b) T. Saito, N. Yamamoto, T. Nagase, T. Tsuboi, K. Kobayashi, T. Yamagata, H. Imoto and K. Unoura, *Inorg. Chem., 29* (1990) 764.
19 G. Hogart, G.A. Phillips, F. Van Gastel, N.J. Taylor, T.B. Marder and A.J. Carty, *J. Chem. Soc., Chem. Commun.,* (1988) 1570.
20 J.K. Burdett and J.H. Lin, *Inorg. Chem. Soc., 21* (1982) 5.
21 (a) F. Cecconi, C.A. Ghilardi, S. Midollini, A. Orlandini and P. Zanello, *Polyhedron, 5* (1986) 2021; (b) E. Diana, G. Gervasio, R. Rossetti, F. Valemarin, G. Bor and P.L. Stangellini, *Inorg. Chem., 30* (1991) 294; (c) D. Fenske, J. Ohmer and J. Hachgenei, *Angew. Chem., Int. Ed. Engl., 24* (1985) 993; (d) D. Fenske, J. Ohmer and K. Merzweiler, *Z. Na-*

turforsch., Teil B, 42 (1987) 803; (e) H. Mao-Chun, H. Zhi-Ying, L. Xin-Jian, W. Guo-Wei, K. Bei-Sheng, L. Han-Qin and J. Huaxnef, *Inorg. Chim. Acta, 159* (1989) 1.

22 (a) A. Bencini, S. Midollini and C. Zanchini, *Inorg. Chem., 31* (1992) 2132; (b) A. Bencini, C.A. Ghilardi, A. Orlandini, S. Midollini and C. Zanchini, *J. Am. Chem. Soc., 114* (1992) 9898.

23 (a) R.G. Woolley, *Inorg. Chem., 24* (1985) 3519; (b) *24* (1985) 3525; (c) D.G. Evans, *Inorg. Chem., 25* (1986) 4602.

24 C. Bianchini, F. Laschi, D. Masi, C. Mealli, A. Meli, F.M. Ottaviani, D.M. Proserpio, M. Sabat and P. Zanello, *Inorg. Chem., 28* (1989) 2552.

25 J.C. Huffman, J.G. Stone, W.C. Krusell and K.G. Caulton, *J. Am. Chem. Soc., 99* (1977) 5829.

26 (a) F. Bottomley, D.E. Paez and P.S. White, *J. Am. Chem. Soc., 107* (1985) 7226; (b) F. Bottomley, D.F. Drummond, D.E. Paez and P.S. White, *J. Chem. Soc., Chem. Commun.,* (1986) 1752.

27 P. Kubacek, P. Hoffmann and Z. Havlas, *Organometallics, 1* (1982) 180.

28 C.G. Arena, F. Faraone, M. Fochi, M. Lanfranchi, C. Mealli, R. Seeber and A. Tiripicchio, *J. Chem. Soc., Dalton Trans.,* (1992) 1847.

29 (a) M. McPartlin, C.E. Eady, B.F.G. Johnson and J. Lewis, *J. Chem. Soc., Chem. Commun.,* (1976) 883; (b) P.F. Jackson, B.F.G. Johnson, J. Lewis, M. McPartlin and W.J.H. Nelson, *J. Chem. Soc., Chem. Commun.,* (1979) 735.

30 M.S. Paquette and L.F. Dahl, *J. Am. Chem. Soc., 102* (1980) 6623.

31 P.H.M. Budzelaar, J. Boersma, G.J.M. van der Kerk, A.L. Spek and A.J.M. Duisenberg, *Organometallics, 4* (1985) 680.

32 K.C.C. Kharas and L.F. Dahl, *Adv. Chem. Phys., 70* (1988) 253.

33 R. Mason, K.M. Thomas and D.M.P. Mingos, *J. Am. Chem. Soc., 95* (1973) 3800.

34 J. Reinhold, E. Hunstock and C. Mealli, *New J. Chem.,* in press.

35 B. Walther, H. Hartung, J. Reinhold, P.G. Jones, C. Mealli, H.-C. Böttcher, U. Baumeister, A. Krug and A. Möckel, *Organometallics, 11* (1992) 1542.

36 (a) C. Mealli, *J. Am. Chem. Soc., 107* (1985) 2245; (b) C. Mealli and D.M. Proserpio, *Comm. Inorg. Chem., 9* (1989) 37.

37 C. Mealli, D.M. Proserpio, G. Fachinetti, T. Funaioli, G. Fochi and P.F. Zanazzi, *Inorg. Chem., 28* (1989) 1122.

38 (a) R. Hoffmann, H. Fujimoto, J.R. Swenson and C.C. Wan, *J. Am. Chem. Soc., 95* (1973) 7644; (b) R. Hoffmann and H. Fujimoto, *J. Phys. Chem., 78* (1974) 1167.

39 S. Alvarez, *Tables of Parameters for Extended Hückel Calculations,* Departamento de Quìmica Inorgànica, Universitat de Barcelona, 1989.